Proc. NIPR Symp. Upper Atmos. Phys., **12**, 12–29, 1998

PROPAGATION OF A QUASI ELECTROSTATIC WHISTLER MODE AURORAL HISS TO THE GROUND

Toshio MATSUO, Toshihiro NISHIYAMA and Daisuke MATUBARA

Graduate School of Informatics, Kyoto University, Sakyo-ku, Kyoto 606-8501

Abstract: It has been thought from ray tracing studies that quasi electrostatic whistler mode auroral hiss is difficult to propagate down to the ground. To evaluate a refracting capability of VLF waves, we use the equations which were originally given by R. R. SCARABUCCI (1969).

The refracting capability becomes gradually large with decreasing altitude in the height range above 2000 km, and it becomes very large by a gradient of electron density below 2000 km.

It is confirmed from ray tracing and the calculation of the refracting capability that the wave normal of a quasi electrostatic whistler mode auroral hiss can enter the transmission cone at the ionospheric altitude when a latitudinally irregular magnetospheric plasma model is adopted, but, such a wave propagation is impossible with a simple diffusive equilibrium (DE) model. As the result, hiss is able to propagate down to the ground under the restricted condition.

1. Introduction

It has been known that VLF emission occurrences in the magnetosphere are closely associated with auroras. Auroral disturbances are often accompanied by intense burst of broad-band radio emissions at frequencies from a few hundred Hz to over 100 kHz (*e.g.*, JORGENSEN and UNGSTRUP, 1962). These emissions observed by satellites and on the ground have been known as auroral hiss, as reviewed by SAZHIN *et al.* (1993).

Auroral hiss observed on the ground are classified into two types. One is the continuous hiss closely associated with a quiet auroral arc, whose frequency range is below 20 kHz (MAKITA, 1979).

MAKITA (1979) reported a relationship between the continuous auroral hiss and auroral luminosity using a large number of data set based on ground observations at Syowa Station (geomag. lat., -70.4°) in Antarctica, in which he pointed out that when auroral arcs appeared in the higher latitude side (south) of Syowa Station, a probability of hiss observation became higher as is shown in Fig. 1.

TANAKA and NISHINO (1988) deduced the exit points of auroral hiss from the ionosphere by a direction finding system installed at Syowa Station (NISHINO *et al.*, 1981), and they concluded that when a quiet auroral arc appeared poleward from Syowa Station, the continuous auroral hiss could penetrate through the ionosphere to the ground after leaking out from duct at an altitude range of 3000–5000 km.

The other type of auroral hiss is the impulsive hiss which has a wide frequency range of lower than 120 kHz (MAKITA, 1979), which is thought to be generated in the localized regions of bright electron auroras. The arrival direction of this type of hiss changes rapidly in accordance with the auroral movements (NISHINO *et al.*, 1981).

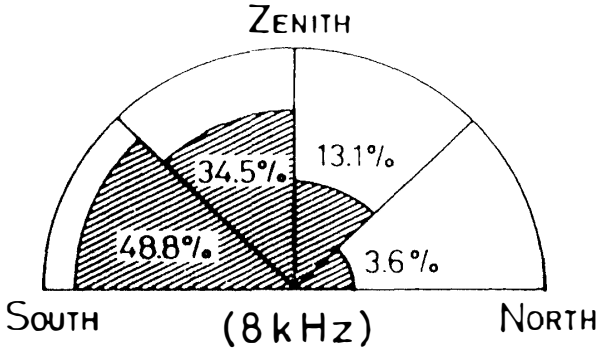

Fig. 1. The relationship between the continuous hiss and the location of aurora at Syowa Station in Antarctica. When auroral arc appeared poleward (South) of Syowa, the probability of hiss observation is very high (after MAKITA, 1979).

The first satellite observation of auroral hiss showed that auroral hiss is closely related with intense fluxes of precipitating electrons with energies less than 10 keV (GURNETT, 1966). Since auroral hiss occurs at frequencies below the local electron gyrofrequency, it is thought to propagate with the whistler mode in the magnetosphere. The downward propagating V-shaped auroral hiss is closely associated with the inverted V electron precipitation, which is observed mainly at low altitudes, below 1 R_E (GURNETT and FRANK, 1972). As auroral hiss is thought to be produced by a Landau resonance (MAGGS, 1976), the electron beam moves in the same direction as the wave.

Recently, KASAHARA *et al.* (1995) demonstrated the propagation vector of the downward propagating auroral hiss measured by PFX instruments on board the Akebono satellite, in which they found that auroral hiss was initially emitted in all directions with a large wave normal angle. The result of the propagation vector analysis is consistent with the theory that auroral hiss is generated by incoherent Cerenkov radiation (MAGGS and LOTKO, 1981) due to precipitating auroral particles. Therefore, auroral hiss propagates from a source region which is thought to be located at around 2–3 R_E along the auroral field line.

Nearly field-aligned propagation in the plasmasphere, such as ducted or prolongitudinally propagation allows a whistler mode to propagate down to the ground because of a small wave normal angle to the vertical. But, for a quasi electrostatic whistler mode wave, penetration through the ionosphere to the ground is rather difficult as is realized by ray tracing studies, and is especially very difficult for poleward propagation. Because the angle between the wave normal direction and vertically downward direction at the wave injection altitude becomes considerably large for the poleward propagation as compared with that for equatorward propagation. Our concern is the propagation of a quasi electrostatic whistler mode auroral hiss to the ground. Why quasi electrostatic VLF waves cannot reach the ground on ray tracing studies? The main reason would be attributed to the kind of electron density model adopted for ray tracing. Namely, if we use the background electron density model with only DE (diffusive equilibrium) (ANGERAMI and THOMAS, 1964), the wave normal is able to become vertically downward for the waves propagating with a small wave normal angle, but this simple model is insufficient for a quasi electrostatic VLF waves.

In the present paper, we study how the wave normal direction of a quasi electrostatic whistler mode wave can be bent downward, and how its wave normal can enter the transmission cone, using by ray tracing technique and the refracting capability calculation. In these calculations, we adopt a model with a field-aligned duct superimposed to

the background DE model. This model refers to ISIS-I topside sounder data taken during the presence of an auroral arc (BENSON and AKASOFU, 1984).

2. Propagation Directions of Auroral Hiss Observed by the Akebono Satellite

Poynting flux analyzers (PFX) onboard the Akebono satellite made it possible to estimate the wave normal directions of auroral hiss. The analyzers measure 2 components of electric fields and 3 components of magnetic fields (KIMURA *et al.*, 1990; HASHIMOTO *et al.*, 1997). The wave normal directions are determined by the wave distribution function (WDF) method (STOREY and LEFEUVRE, 1979), using these 5 components of the electric and magnetic field data. It is well known that the maximum entropy (MEM) (LEFEUVRE and DELANNOY, 1979) and Phillips–Tikhonov regularization method (PTM) (YAMAGUCHI *et al.*, 1994) are suitable for the analysis of hiss type emissions (KASAHARA *et al.*, 1995), but MEM is available for the assumption of one source (region and) with no additional noise.

In the present paper, we use the PTM method to determine the wave normal direction of auroral hiss which may have multiple source region.

Figure 2 displays the dynamic spectra of auroral hiss observed by Akebono at an altitude around 8000 km during 0242–0254 UT on June 26, 1991. The wave normal angle (ψ) at the frequency of 10.2 kHz determined by PTM is plotted in Fig. 3. In this figure, the center of the left circle denotes the direction of the geomagnetic field, and polar angle (ψ) is given by a radial distance from the center, and the circumference of the circle denotes the azimuthal angle (φ). From this figure, it is found that the wave

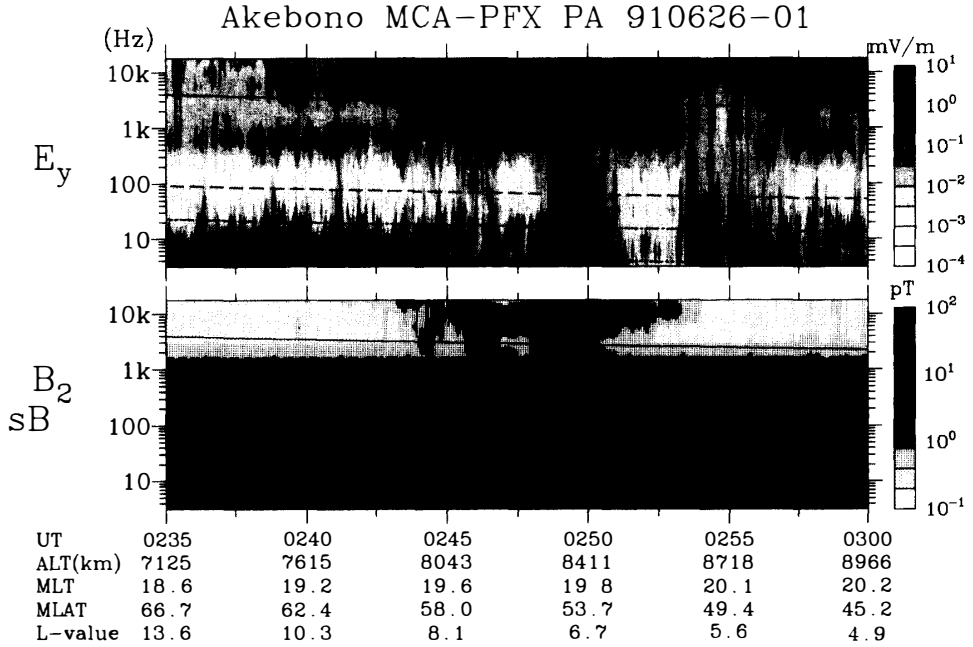

Fig. 2. Upper and lower panel shows the dynamic spectra of V-shaped auroral hiss by the electric and the magnetic sensors respectively, observed on June 26, 1991 by MCA (Multi Channel Analyzer) onboard the Akebono (EXOS-D) satellite.

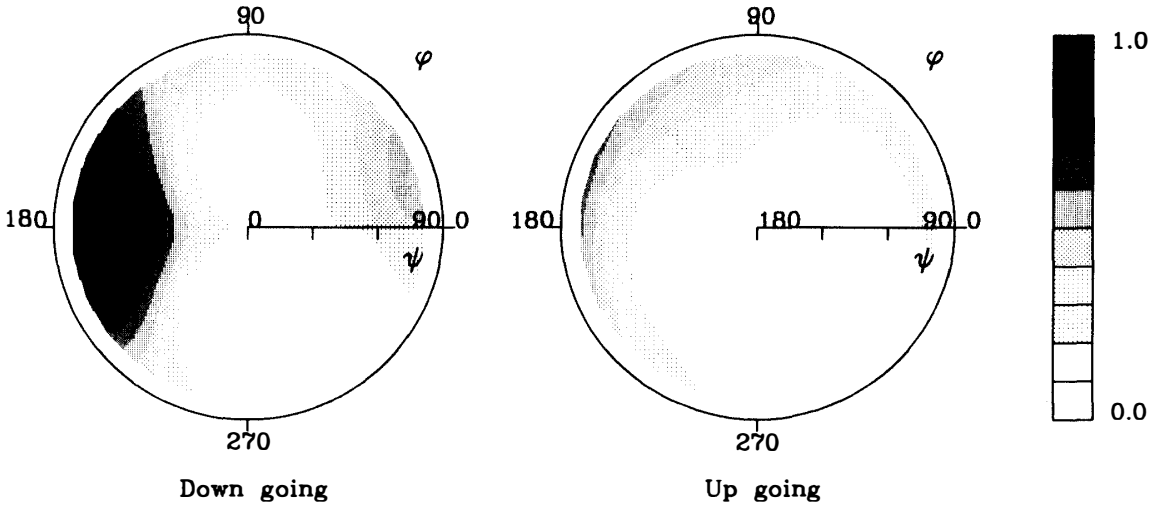

Fig. 3. The wave normal direction of V-shaped auroral hiss at the frequency of 10.2 kHz observed on June 26, 1991 at 0249:02(UT).

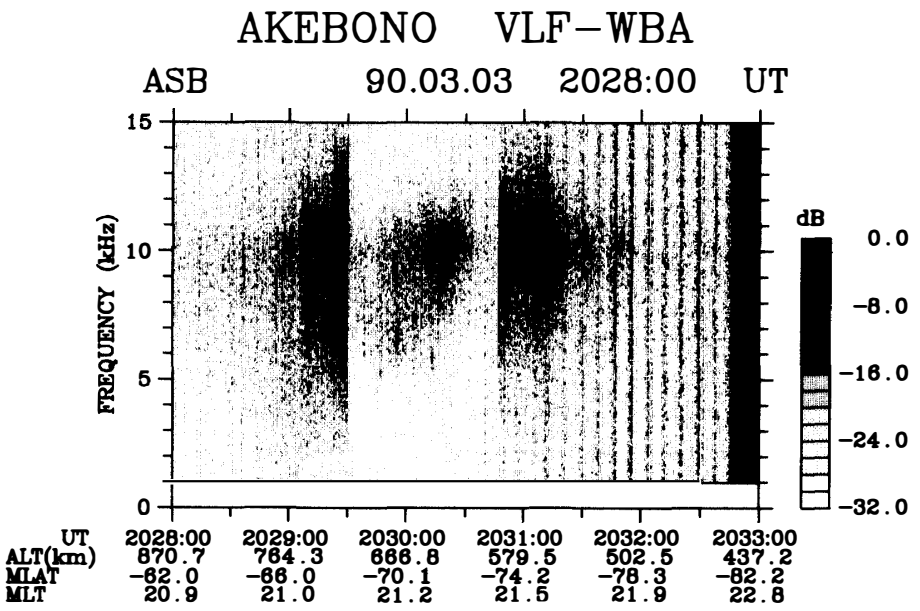

Fig. 4. A frequency-time spectrogram of V-shaped auroral hiss observed on March 3, 1990. The data was taken at Syowa tracking station.

normal direction is directed downward with $\psi \sim 72^\circ$ and $\varphi \sim 180^\circ$, which is close to the resonance cone angle around an altitude of 8400 km.

On the other hand, we also measured ψ of auroral hiss which was observed at low altitudes. The frequency spectrogram shown in Fig. 4 represents the V-shaped auroral hiss observed at an altitude range of 500–700 km in the geomagnetic latitude range from -65° to -78° on March 3, 1990, where the gain of the VLF wideband receiver was reduced by 25 dB during the time period of 2029:30–2030:45. The wave normal direction is estimated from PFX data, whose center frequency was 9 kHz$\pm$50 Hz as shown in Fig. 5. The wave normal direction is definitely downgoing in the southern hemisphere, and its angle (ψ) is considerably small, compared with that of 8400 km

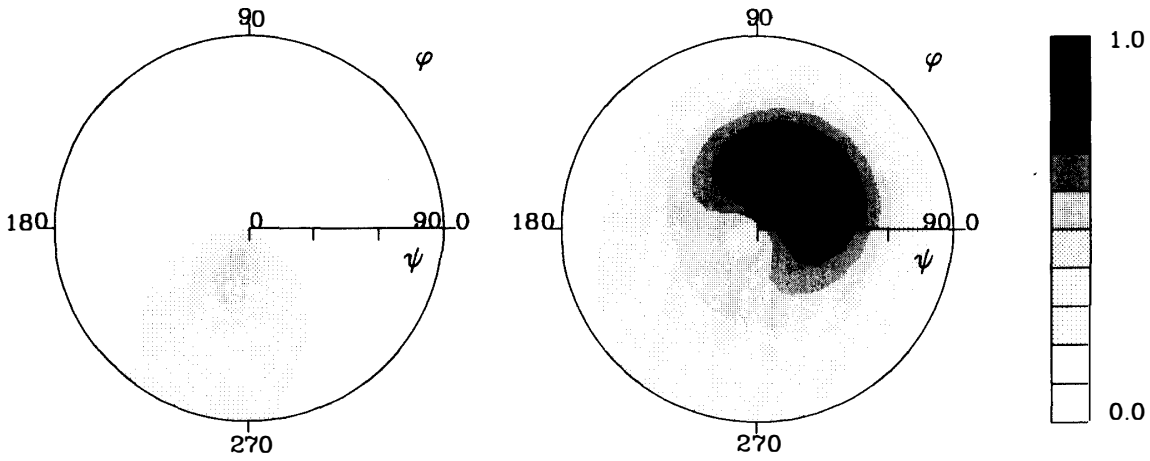

Fig. 5. The wave normal direction of V-shaped auroral hiss at the frequency of 9 kHz observed on March 3, 1990 at 2030:04 (UT) at an altitude of 660 km.

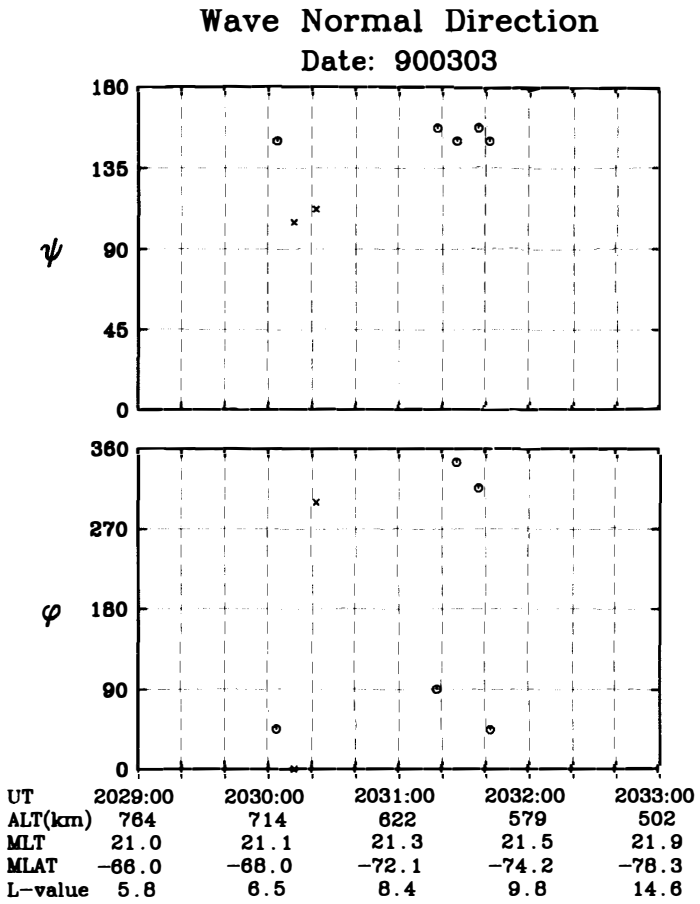

Fig. 6. Latitudinal dependence of the wave normal angles of auroral hiss at an altitude of 500–700 km observed on March 3, 1990.

altitudes shown in Fig. 3. Figure 6 represents the latitudinal dependence of the wave normal directions observed on March 3, 1990. In this case, the frequency of PFX is swept every 7.5 s like stairs in the frequency range of 1–11 kHz, as shown in Fig. 7.

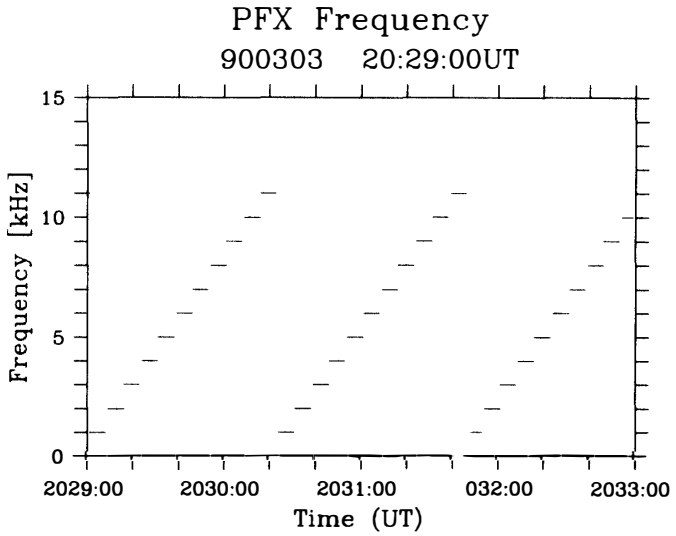

Fig. 7. PFX step frequencies from 1 to 11 kHz every 7.5 s on March 3, 1990.

Therefore the wave normal direction plotted in Fig. 6 are for different frequencies. Seven points were successfully analyzed above 8 kHz. It is found that 5 out of 7 points indicate the propagation nearly along the auroral field lines in the geomagnetic meridian plane as shown by ○, and remaining 2 indicate large wave normal angles.

3. Propagation Vector of Auroral Hiss by Ray Tracing Studies

3.1. Electron density model in a polar magnetosphere

BURTIS (1974) developed an electron density model which is composed of a factor representing a duct and a factor representing the plasmapause. In particular, the main features of this duct model are that it takes account of the altitude of the duct base, and also the duct enhancement factor ($c(k)$ in the following equation) is continuously reduced to merge into the background density below the bottom of the duct. Namely, this electron density model (N_e) is expressed as follows,

$$N_e = N_{e0} \cdot N_{DE} \cdot N_{LI} \cdot N_{pp} \cdot N_{duct} , \tag{1}$$

where N_{e0} is the density at the reference altitude (1000 km) by the diffusive equilibrium (DE) model developed by ANGERAMI and THOMAS (1964). N_{DE} and N_{pp} are the factor depending the diffusive equilibrium and the plasmapause respectively, and N_{LI} is the factor depending the lower ionosphere. N_{duct} is the duct factor which is able to represent multiple k ducts, as is expressed as follows.

$$N_{duct} = \prod_{k=1}^{m} \cdot \left[1 + c(k) \cdot \exp\left\{ -\left(\frac{1}{2}\right) \frac{(L - L_0(k))^2}{\Delta L^2(k)} \right\} \cdot F_{ducted} \right] , \tag{2}$$

where

$$\left.\begin{aligned} F_{ducted} &= \exp\left\{ -\frac{(r_e(k) - r)^2}{r_g^2(k)} \right., \quad \text{for} \quad r < r_e \\ &= 1, \quad \text{for} \quad r > r_e \end{aligned}\right\} \tag{3}$$

and $c(k)$, $L_0(k)$ and $\Delta L(k)$ are the enhancement factor, the duct center (in L) and the half width (in L) of the k^{th} duct, respectively. $r_e(k)$ is the geocentric distance (km) of the bottom of the k^{th} duct.

To understand the influences of the background plasma configuration, we use two magetospheric plasma models; one is a DE model which includes only an effect of radial density gradient, and the other model includes also a latitudinal dependence of radial density gradient. $r_g(k)$ is the radial scale height of the bottom of the k^{th} duct.

3.2. *Wave normal variations for a simple DE model*

To investigate whether or not a quasi electrostatic aurora hiss can penetrate the ionosphere, we calculated by ray tracing (KIMURA, 1966) how its wave normal angles vary with decreasing altitude. In this calculation, as is shown in Fig. 8, the positive direction of the geomagnetic field is taken to be upward, and when the wave normal direction (ψ) is measured anti-clockwise from the positive direction of geomagnetic field, it is positive. The angle δ is positive when it is measured anti-clockwise from the radially upward direction. Figure 8 shows schematically the relation between the location of aurora and the propagation direction of auroral hiss. When a wave is injected poleward, it propagates toward higher latitudes than the latitude of auroral appearance.

Figure 9 represents altitude dependence of ray paths and the wave normal directions by ray tracing using the DE model. The gray scale represents the contour map of electron density, calculated with a simple DE model including plasmapause. The relative

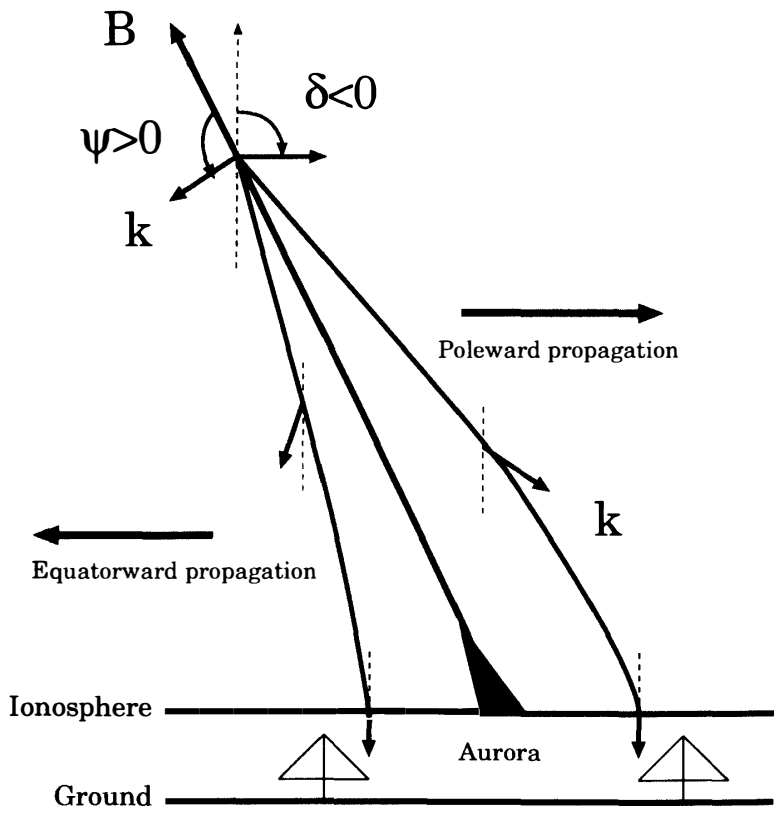

Fig. 8. Schematic diagram showing the propagating direction of auroral hiss and the location of aurora.

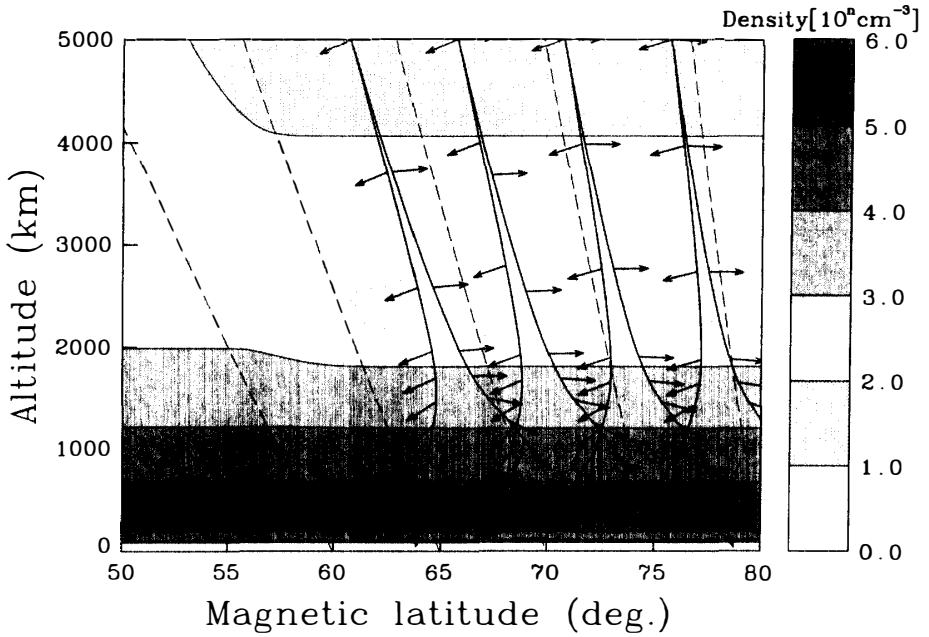

Fig. 9. The altitude dependence of the ray paths and the wave normal directions calculated by ray tracing under a simple DE model. The initial wave normal angle of 5 kHz waves are taken to be the resonance cone angle −10° at an altitude of 5000 km regardless of the propagating directions. Each arrow and the contour map drawn by the gray scale show the wave normal directions and the electron density distribution in the background based on the DE model.

concentration ratio of three major ions, H^+, He^+ and O^+, to the electron density (N_{e0} at a reference level of 1400 km), and electron temperature T_e were taken to be 0.01, 0.09, 0.9 and 1500 K respectively. The electron density below an altitude of 2000 km ranges 10^3–10^5 cm^{-3}, with a considerably large density gradient as compared with that on a quiet period of no aurora.

We calculated the ray paths for 5 kHz waves emitted poleward and equatorward in the geomagnetic meridian plane with the initial wave normal angles of the resonance cone angle minus 10° in the latitude range of 60°–75° at an altitude of 5000 km. The arrows and the downward solid lines represent the wave normal directions and ray paths respectively, and the broken lines represent the magnetic field lines. The wave normal angles for each ray are almost unchanged above an altitude of 2000 km. Even below an altitude of 2000 km, all wave normals are not sufficiently bent toward the vertically downward direction. This tendency is almost the same for hiss propagating equatorward or poleward. Especially for poleward propagation, as the angles between the wave normal and the vertically downward are larger than that for equatorward one, it is considerably difficult for the wave propagating poleward to be bent vertically downward at the ionospheric altitude. Therefore, a larger radial gradient of electron density is required for the wave normal to enter the transmission cone.

3.3. Wave normal variations for irregular polar magnetospheric plasma model

To investigate how a quasi electrostatic whistler mode auroral hiss is able to propagate down to the ground, we examine here the case with an irregular polar magnetospheric plasma model, which is constructed from ISIS–I topside sounder data at

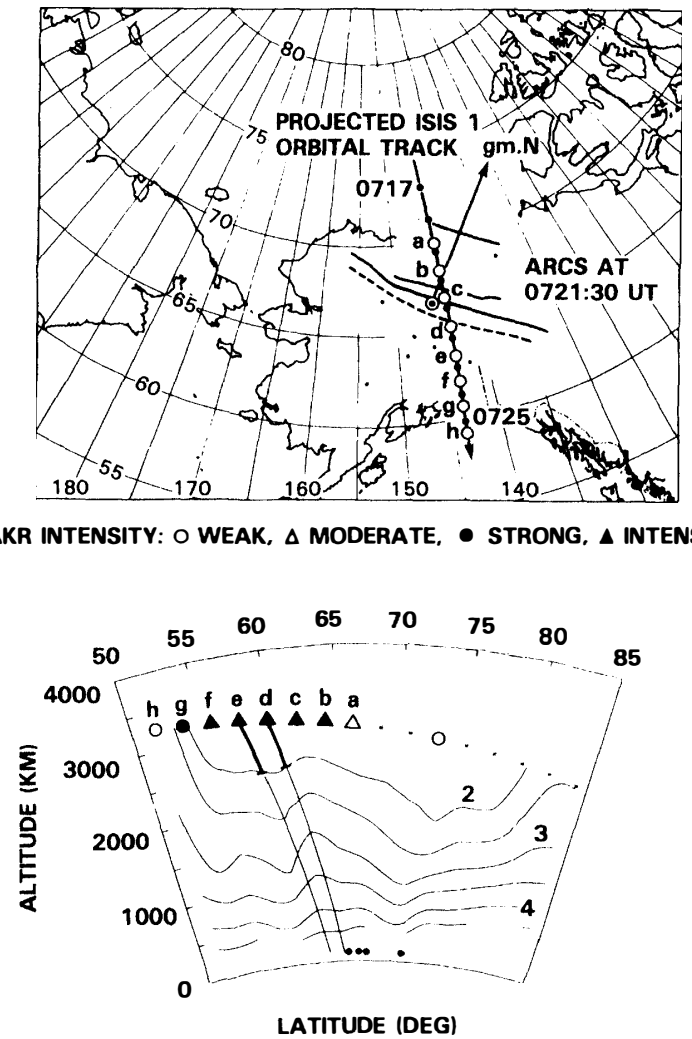

Fig. 10. Upper panel shows ISIS-I orbital track (projected along B to 100 km altitude) and location of multiple auroral arc. Lower panel are electron density contours corresponding to the value 10^2, 10^3, 10^4 from the satellite position down to the F layer peak density. Four small black dot around an altitude of 100 km represents location of multiple auroral arc (After BENSON *and* AKASOFU, *1984).*

the time of auroral arc appearance (BENSON and AKASOFU, 1984). BENSON and AKASOFU demonstrated a relationship between electron density contour map (with AKR information) by ISIS–I and locations of multiple auroral arcs by all sky camera images as is shown in Fig. 10. In this figure, the arc appearance looks like to cause a latitudinal change in electron density. Energetic electrons penetrated into the upper atmosphere produce aurora luminescence, and at the same time they cause the electron density enhancement.

With ray tracings for two models, we tried to see how the ray path and the wave normal direction change depending upon these background plasma structure. First, we examined a moderately disturbed model at the time of the stable auroral arc appearance.

Upper panel in Fig. 11 shows the altitude dependence of ray paths and their wave normal directions for the equatorward injection at 5000 km altitude. The initial conditions for wave injections are assumed to be the same as the case in the simple DE model

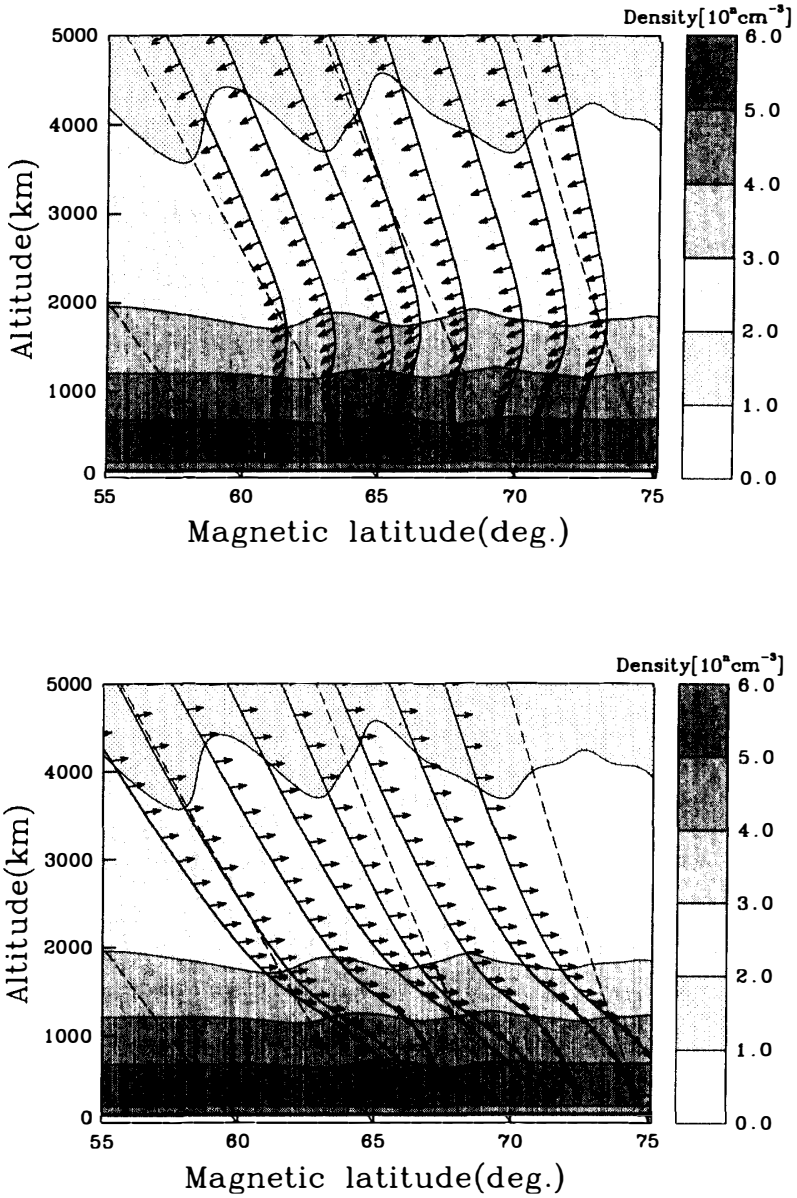

Fig. 11. The calculation same as in Fig. 9 was done for moderately disturbed plasma model. Upper and lower panels show an altitude dependence of the ray path and the wave normal angle of 5 kHz waves injected into equatorward and poleward respectively, whose initial wave normal angle is assumed to be the resonance cone angle $-10°$.

shown in Fig. 9. The parameters in a moderately disturbed model are taken to be the same condition as a simple DE model except the parameters for multiple ducts in eq. (2). Table 1 shows the parameters of multiple ducts. The contour map shown by the gray scale represents the spatial electron density distribution. It is clearly seen that the wave normal angles (ψ) of each ray change a little for an altitude range of 2000–5000 km, but below 2000 km altitude, they are bent noticeably downward by the additional effect of the latitudinal density gradient, so that the wave normals direct nearly downward. For the poleward wave injection, as is shown in lower panel, ψ shows the similar behavior to those of the equatorward wave injection for an altitude range of

Table 1. Parameters for the moderately disturbed electron density model.

k	$L_0(k)$	$\Delta L(k)$	$c(k)$	$r_c(k)$	$r_g(k)$
1	4.0	0.	0	6370+1000	300
2	4.5	2.0	−0.2	6370+1000	300
3	5.0	2.0	0.2	6370+1000	300
4	5.5	0.4	−0.3	6370+1000	600
5	6.5	0.6	0.25	6370+1000	3000
6	7.5	0.5	−0.25	6370+1000	1000
7	9.6	0.5	0.3	6370+1000	300
8	13.0	1.0	−0.2	6370+1000	100
9	18.5	1.0	0.1	6370+1000	300
10	25.0	1.0	−0.1	6370+1000	300
11	30.0	1.0	−0.2	6370+1000	100
12	40.0	0.5	0.2	6370+1000	300

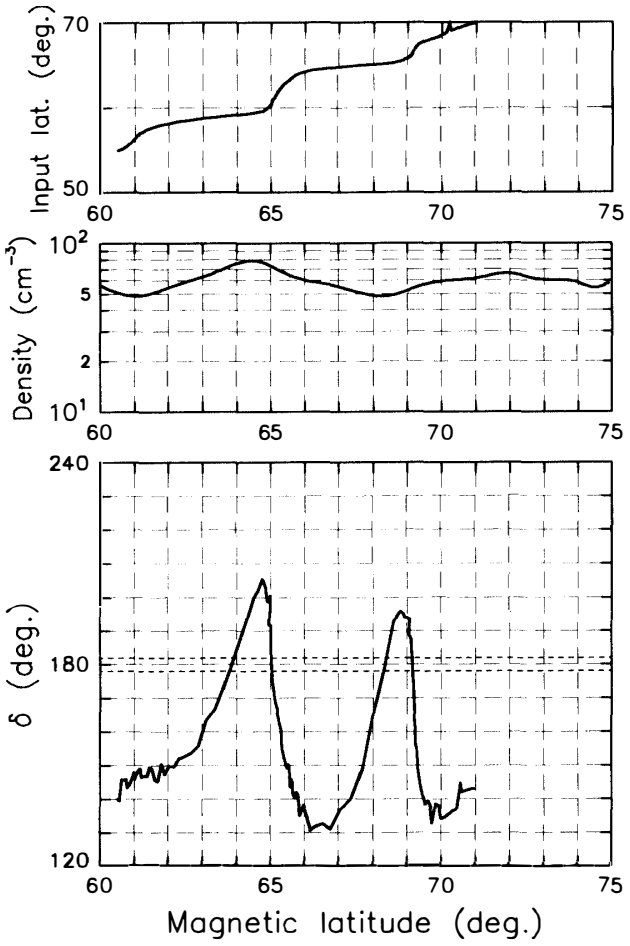

Fig. 12. The top panel shows a magnetic latitude characteristics of equatorward wave input (5000 km) −output (200 km). The middle panel shows a latitudinal dependence of electron density at an altitude of 5000 km by moderately disturbed model. The bottom panel shows a latitudinal variation of the wave normal angle from radial direction at an altitude of 200 km.

2000–5000 km, but it shows a different behavior below 2000 km of altitude in comparison with those of the upper panel. As the angle between the initial wave normal and the vertically downward direction becomes larger in comparison with that of the equatorward injection, most of the cases, ψ are still large angles with respect to the radially downward direction at the ionospheric altitude, but some rays are able to enter the transmission cone.

To ascertain whether or not the wave normal of auroral hiss is able to enter the transmission cone, we calculated the wave normal angle from the radially upward direction (δ shown in Fig. 8) at an altitude of 200 km. Calculations for the equatorward propagation were carried out under the same conditions as the upper panel in Fig. 11. The ray paths were calculated every 0.1° from 55–70° (Mlat.). The top panel in Fig. 12 shows the relationship of wave injection magnetic latitudes (at 5000 km altitude) in the ordinate with output latitudes (at 200 km) in the abscissa. The middle panel shows the latitudinal dependence of electron density at an altitude of 5000 km. The bottom panel shows a latitudinal dependence of δ at an altitude of 200 km. In the bottom panel, dotted lines of $180^\circ \pm 2^\circ$ represent the transmission cone angle. For such an equatorward wave injection, δ of auroral hiss is within the transmission cone at about 63.8, 65.0, 68.3 and 69.2° (Mlat).

For the poleward wave injection, the penetrating condition is severer as compared with that of the equatorward wave injection, but δ becomes within $180^\circ \pm 2^\circ$ transmission cone at about 67° and 68.2° (Mlat.) (not shown).

Secondly, we tried calculations of the ray path and ψ for a disturbed electron density model, which was reproduced from the ISIS-I topside sounder data during the presence of an Ω band aurora. It shows an extremely sharp latitudinal gradient of electron density (BENSON and AKASOFU, 1984). The parameters of this disturbed electron density are the same as the moderately disturbed model except the parameters of ducts. Table 2 shows parameters for a disturbed model. The width ($\Delta L(k)$) and the enhancement factor ($c(k)$) of the k^{th} duct are taken to be narrower and higher than those of the moderately disturbed electron density model in Table 1. Figure 13 shows the

Table 2. Parameters for the disturbed electron density model.

k	$L_0(k)$	$\Delta L(k)$	$c(k)$	$r_e(k)$	$r_g(k)$
1	3.7	0.2	0.0	6370+1000	300
2	4.3	0.15	0.6	6370+1000	3000
3	4.7	0.1	0.0	6370+1000	300
4	5.1	0.3	0.3	6370+1000	1000
5	5.6	0.2	−0.8	6370+1000	500
6	6.0	0.2	0.6	6370+1000	3000
7	7.8	0.2	−0.7	6370+1000	500
8	7.8	0.4	0.7	6370+1000	3000
9	8.5	0.4	−0.65	6370+1000	600
10	10.4	0.6	0.85	6370+1000	3000
11	13.1	0.5	−0.6	6370+1000	1000
12	14.9	0.5	0.2	6370+1000	300
13	17.1	1.0	−0.2	6370+1000	100
14	19.7	1.5	0.2	6370+1000	300

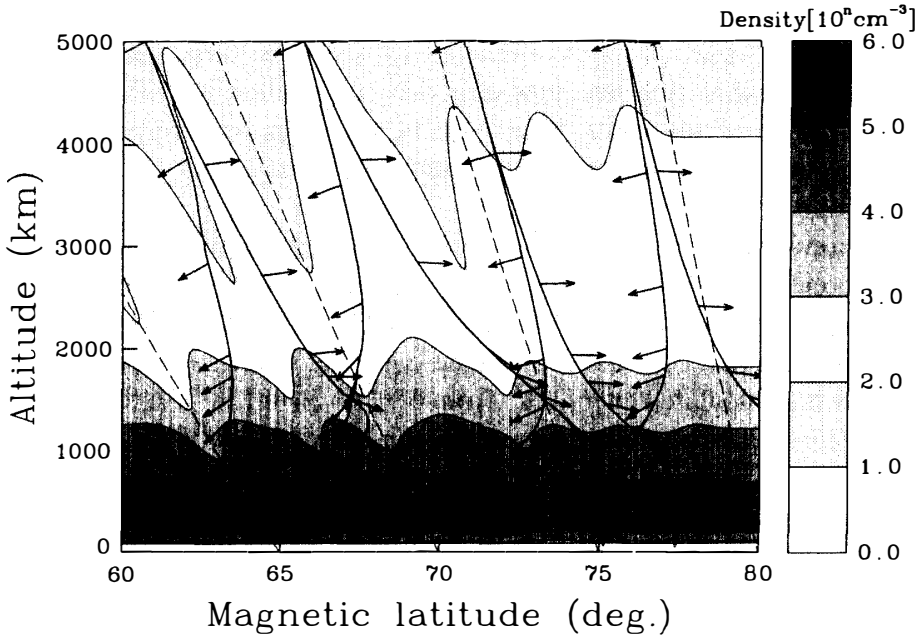

Fig. 13. The altitude dependence of the ray paths and the wave normal angles for equatorward and poleward wave injection, respectively.

ray paths for the equatorward and poleward wave injection respectively. The behavior of the wave normal angles for an altitude range of 2000–5000 km are similar to those shown in Fig. 11, but below 2000 km altitude, the wave normal directions are violently rotated by the effect of sharp latitudinal density gradient. Therefore, it is rather difficult for the wave normal directions to enter into the transmission cone. But, though they are not shown here, some rays are still able to propagate down to the ground by the similar analysis.

4. Wave Normal Direction and the Refracting Capability

4.1. Relationship between ψ and $\partial\psi/\partial t$

According to SCARABUCCI (1969), the time variation of wave normal angle is governed by the following equation.

$$\frac{2n}{c}\frac{\partial\psi}{\partial t} = -\sin\delta\left\{\frac{1}{N_e}\frac{\partial N_e}{\partial r} + \frac{3}{r}(M_c + M_y)\right\} + \frac{\cos\delta}{r}\left\{\frac{1}{N_e}\frac{\partial N_e}{\partial\theta} + M_\theta\right\}, \qquad (4)$$

where n is the refractive index. ψ and δ are defined as shown in Fig. 8. The direction of the magnetic field is assumed to be upward. N_e is the electron density, r is the geocentric radius, θ is the colatitude and t is the time in second. The factor M_c, which expresses the influence of the curvature of the geomagnetic field is given by

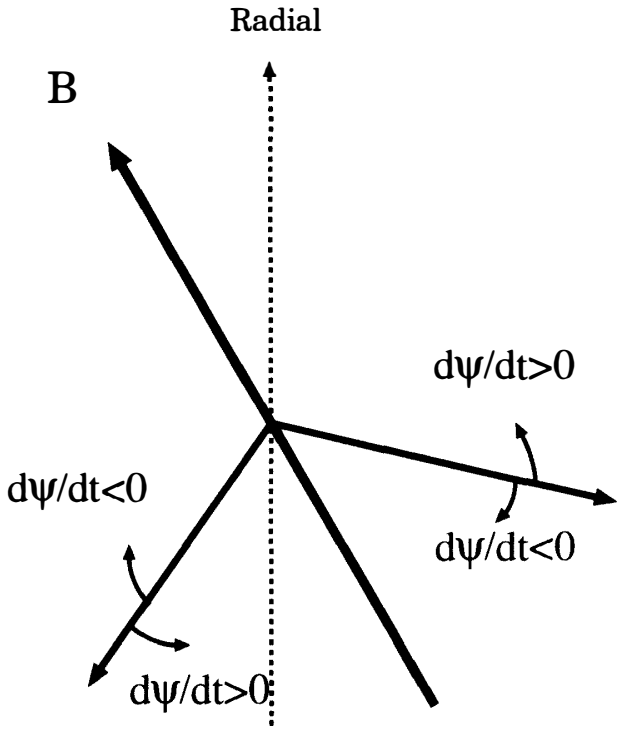

Fig. 14. Schematic diagram showing the polarity of the refracting capability and the rotation of the wave normal angle.

$$M_c = \frac{2(1+\cos^2\theta)}{1+3\cos^2\theta}, \tag{5}$$

and both the terms M_y and M_θ, the influence of the gradient of magnetic field intensity are given by

$$M_y = \frac{\cos\psi}{\cos\psi - f/f_{He}}, \tag{6}$$

$$M_\theta = \frac{3\sin\theta\cos\theta}{1+3\cos^2\theta}\cdot M_y, \tag{7}$$

where f_{He} is the electron cyclotron frequency.

As is shown in Fig. 14, when the derivative of ψ with respect to t in eq. (4) is positive, the wave normal is bent anti-clockwise, as the angle ψ is measured to be positive as shown in Fig. 8. This equation was first adopted by EDGAR (1976) to explain a large positive and negative doppler shift of man-made VLF signals.

4.2. Altitude dependence of the refracting capability and the wave normal direction

We calculated the right hand side of eq. (4) to understand how the refracting capability works so as to make the wave normal direction bent into transmission cone at the ionospheric level. Equation (4) is divided into two parts. Namely, K_N is the term representing the density gradient, and K_B is the term dependent on the geomagnetic field.

$$K_N = -\sin\delta\cdot\frac{1}{N_e}\cdot\frac{\partial N_e}{\partial r} + \frac{\cos\delta}{r}\cdot\frac{1}{N_e}\cdot\frac{\partial N_e}{\partial\theta}, \tag{8}$$

$$K_B = -\sin\delta \cdot \frac{3}{r} \cdot (M_c + M_y) + \frac{\cos\delta}{r} \cdot M_\theta , \tag{9}$$

$$\frac{2n}{c}\frac{\partial\psi}{\partial t} = K_N + K_B . \tag{10}$$

As the wave normal direction is strongly controlled by the polarity and the magnitude of eq. (4) or eq. (10), we calculate K_N, K_B and $2n/c \cdot (\partial\psi/\partial t)$ to check the effects of the refracting capability. Hereafter, $2n/c \cdot (\partial\psi/\partial t)$ of eq. (4) is called the refracting capability.

Figure 15a shows the altitude dependence of K_N, K_B and $2n/c \cdot (\partial\psi/\partial t)$ along the ray path for the poleward injection at 70° geomagnetic latitude by the simple DE model, where these quantities are represented by the dashed, dotted and solid lines respectively. As is clearly shown, the magnetic field dependent term K_B takes small positive values all over the altitude range concerned. The positive K_B means to make the wave normal bent slightly anti-clockwise. The polarity of K_N is negative above the altitude of 300 km. In

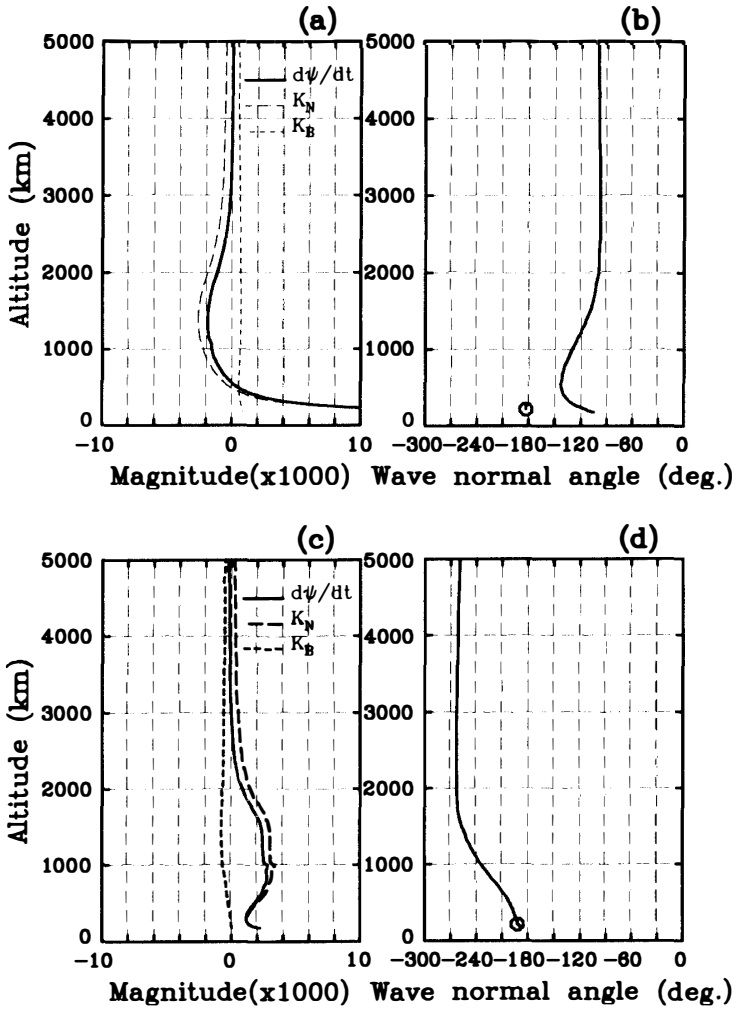

Fig. 15. Altitude dependence of the refracting capabilities and the wave normal angles. Top panel allow for the poleward injection at 70° MLAT by the DE model, and the bottom for the equatorward injection at 60.6° MLAT by the moderately disturbed plasma model, respectively. ○ denote the transmission cone angle at the altitude of 200 km.

the altitude range of 3500–5000 km, as $2n/c \cdot (\partial\psi/\partial t)$ takes a small positive values, for poleward wave injection, the wave normal direction slightly rotates approaching to the negative direction of the geomagnetic field.

In an altitude range of 300–3500 km, K_N and therefore $2n/c \cdot (\partial\psi/\partial t)$ takes large negative values with decreasing altitude, so that ψ is continuously bent approaching to the direction of the geomagnetic field. Below 300 km of altitude, the polarity of $2n/c \cdot (\partial\psi/\partial t)$ becomes positive, and its magnitude abruptly increases with decreasing altitude.

Therefore, from the altitude of 3500 to 300 km, the wave normal direction approaches to the negative direction of the geomagnetic field with decreasing altitude, but below 300 km the wave normal angle (ψ) cannot reach $\psi = -185^\circ$ corresponding to the transmission cone angle, denoted by ○ in Fig. 15b. Because the refracting capability which bends ψ to the vertically downward direction is not enough for simple DE model. For the equatorward injection, the wave normal direction does not also enter the transmission cone by the lack of the refracting capability although the figure is not shown here.

Next, on the moderately disturbed model, a similar calculation results in Figs.15c and d for the equatorward injection from 60.6° (Mlat.). As the polarities of K_N, K_B and $\partial\psi/\partial t$ depend upon the direction of wave normal, the polarity of quantities in Fig. 15c is reversed, in a contrast with Fig. 15a. As the polarity of the refracting capability (the solid line) in Fig. 15c becomes positive below an altitude of 3000 km, ψ is continuously bent toward the negative direction of the geomagnetic field line from 3000 km to the lower ionosphere. The wave normal directs vertically downward ($\psi = -193^\circ$) at an altitude of 200 km by the effect of large refracting capability. Therefore, for the moderately disturbed model, for the equatorward wave injection, the hiss is able to propagate down to the ground.

For the poleward injection, it is found by the detailed calculation (not shown) that the wave normal direction can enter the transmission cone only for the initial wave injection latitude around 58°. Therefore, the possibility of ionospheric penetration of auroral hiss is much less for poleward injection than for equatorward injection.

5. Summary and Discussion

MAKITA (1979) reported that the continuous hiss occurrence is closely associated with the steady auroral arc located at the poleward region of Syowa, in which he clarified that the probability of hiss observation is high when the auroral arcs appear poleward. But, he did not theoretically explain how auroral hiss with a large initial wave normal angle propagates down to the ground. For the equatorward injection of downgoing auroral hiss, the angle between the wave normal and the vertically downward direction becomes smaller than that of poleward wave injection. This implies that if the angle is larger, a larger refracting capability is required for the entrance into the transmission cone at the low ionospheric altitude. Therefore, observation probability is thought to become very low for poleward injection in comparison with the equatorward injection. TANAKA and NISHINO (1988) reported that the continuous hiss emerging from duct can propagate to the ground. But, they did not demonstrate how hiss can propagate in a duct. For a quasi electrostatic whistler mode VLF wave, the refracting

capability of ducts is insufficient owing to a large wave normal angle, so that the duct does not always work as a wave guide for the auroral hiss even if the enhancement factor is large.

We have made clear through the propagation vector analysis of auroral hiss observed on board the Akebono satellite that the auroral hiss in the higher altitude region propagates in the quasi electrostatic whistler mode, but it propagates with a small wave normal angle below 1000 km of altitude. This suggests that there must be a mechanism to bend strongly the wave normal toward the vertically downward direction in lower altitudes, especially below an altitude of 2000 km. It was found by ray tracing and estimation of the refracting capability that the wave normal could not be bent toward vertically downward by only the radial density gradient in the simple DE model.

If, however, an irregular polar magnetospheric plasma model is assumed, there might be a possibility for hiss to propagate down to the ground. To confirm this possibility, we prepared a model with latitudinally irregular electron density variations for ray tracing. One is a moderately disturbed model associated with a stable arc, whose electron density gradient is latitudinally moderate, and the other is a disturbed model with severe auroral disturbances, whose latitudinal density gradient is great.

As the result of ray tracing, under the moderately disturbed model, it is found that the wave normals for the equatorward injection are greatly bent downward by the effect of the latitudinal density gradient, and most of the wave normal direct eventually downward to penetrate the ionosphere to the ground. For the poleward injection, despite of the existence of large refracting capability, the condition for ionospheric penetration of auroral hiss is quite limited in comparison with the equatorward injection. These results are consistent with the observational results (MAKITA, 1979) that auroral hiss is observed when aurora arc appears poleward, *i.e.*, for the equatorward injection, the hiss is able to penetrate through the ionosphere with high probability.

On the other hand, for the disturbed model, it is found that in most cases, the wave normal is too much rotated by the sharp latitudinal density gradient for the equatorward and the poleward propagations, so that the wave normal directions do not, in most of the case, fall into the transmission cone. Although in a restricted condition, some rays are able to propagate down to the ground (not shown) due to a very steep density gradient.

Whether the wave normal direction can enter the transmission cone is strongly dependent on the configuration of the magnetospheric plasma. Therefore, in order to carry out more realistic ray tracing, a simultaneous ground and satellite observation is essential. It is especially important to perform the simultaneous measurement of the spatial distribution of electron density and ground observation of hiss at the time of auroral arc appearance.

Acknowledgments

We would like to greatly thank Prof. I. KIMURA of Osaka Institute of Technology for helpful suggestions and discussions. We would like to thank Prof. K. TSURUDA of Institute of Space and Astronautical Science. We are grateful to the Akebono tracking team members for continual data acquisition of the Akebono telemetry. We are also grateful to Prof. N. SATO, Associate Prof. H. YAMAGISHI, Drs. M. KIKUCHI and M.

OKADA of National Institute of Polar Research for their kind supports to perform this work.

References

ANGERAMI, J. J. and THOMAS, J. O. (1964): Studies of planetary atmospheres, 1. The distribution of electrons and ions in the earth's exosphere. J. Geophys. Res., **69**, 4537–4560.

BENSON, R. F. and AKASOFU, S. (1984): Auroral kilometric radiation and/aurora correlation. Radio Sci., **19**, 527–541.

BURTIS, W. J. (1974): User's guide to the Stanford VLF ray tracing program. Stanford Univ. Tech. Rep., No. 3418–1, Stanford Radio Sci. Lab.

EDGAR, B. C. (1976): The theory of VLF doppler signatures and their relation to magnetospheric density structure. J. Geophys. Res., **81**, 3327–3339.

GURNETT, D. A. (1966): A satellite study of VLF hiss. J. Geophys. Res., **71**, 5599–5615.

GURNETT, D. A. and FRANK, L. A. (1972): VLF hiss and related plasma observations in the polar magnetosphere. J. Geophys. Res., **77**, 172–190.

HASHIMOTO, K., NAGANO, I., YAMAMOTO, M., OKADA, T., KIMURA, I., MATSUMOTO, H. and OKI, H. (1997): EXOS-D (AKEBONO) very low frequency plasma wave instruments (VLF). IEEE Trans. Geosci. Remote Sensing, **35**, 278–286.

JORGENSEN, T. S. and UNGSTRUP, E. (1962): Direct observation of correlation between aurorae and hiss in Greenland. Nature, **194**, 462–463.

KASAHARA, Y., YOSHIDA, K., MATSUO, T. and KIMURA, I. (1995): Propagation characteristics of auroral hiss observed by Akebono satellite. J. Geomagn. Geoelectr., **47**, 509–525.

KIMURA, I. (1966): Effects of ions on whistler-mode ray tracing. Radio Sci., **1.1** (New Series), No. 3, 269–283.

KIMURA, I., HASHIMOTO, K., NAGANO, I., OKADA, T., YAMAMOTO, M., YOSHINO, T., MATSUMOTO, H., EJIRI, M. and HAYASHI, K. (1990): VLF observations by the Akebono (EXOS-D) satellite. J. Geomagn. Geoelectr., **42**, 459–478.

LEFEUVRE, F. and DELANNOY, C. (1979): Analysis of random electromagnetic wave field by a maximum entropy method. Ann. Telecommun., **34**, 204–213.

MGGS, J. E. (1976): Coherent generation of VLF hiss. J. Geophys. Res., **81**, 1707–1724.

MGGS, J. E. and LOTKO, W. (1981): Altitude dependence model of the auroral beam and beam-generated electrostatic noise. J. Geophys. Res., **86**, 3439–3447.

MAKITA, K. (1979): VLF-LF Hiss emissions associated with aurora. Mem. Natl Inst. Polar Res., Ser. A, **16**, 49–56.

NISHINO, M., TANAKA, Y., IWAI, A. and HIRASAWA, T. (1981): A new direction finding technique for auroral VLF hiss based on the measurement of time differences of arrival at three spaced observing points. Planet. Space Sci., **29**, 365–375.

SAZHIN, S. S., BULLOUGH, K. and HAYAKAWA, M. (1993): Auroral hiss: A review. Planet. Space Sci., **41**, 153–166.

SCARABUCCI, R. R. (1969): Interpretation of VLF signals observed on the OGO-4 satellite. Stanford Univ. Tech. Rep., No. 3418–2, Stanford Radio Sci. Lab.

STOREY, L.R.O. and LEFEUVRE, F. (1979): The analysis of 6-component measurements of a random electromagnetic wave field in a magnetoplasma, 1. The direct problem. Geophys. J. R. Astron. Soc., **56**, 255–269.

TANAKA, Y. and NISHINO, M. (1988): The propagation of auroral hiss observed on the ground as deduced from direction finding measurements. Planet. Space Sci., **36**, 259–269.

YAMAGUCHI, M., HATTORI, N., IWAMA, N. and HAYAKAWA, M. (1994): A new direction finding method of magnetospheric VLF/ELF radio waves using the linear regularization and generalized cross validation. Dusty and Dirty Plasma, Noise, and Chaos in Space and in the Laboratory, ed. by H. KIKUCHI. New York, Plenum Press, 405–414.

(Received February 3, 1998; Revised manuscript accepted June 5, 1998)